European Journal of Pharmaceutics and Biopharmaceutics 142 (2019) 195–203

Contents lists available at ScienceDirect

European Journal of Pharmaceutics and Biopharmaceutics

journal homepage: www.elsevier.com/locate/ejpb

Research paper

Light sheet fluorescence microscopy *versus* confocal microscopy: in quest of a suitable tool to assess drug and nanomedicine penetration into multicellular tumor spheroids

Gianpiero Lazzari[a], Daniele Vinciguerra[a,1], Anna Balasso[a,1], Valerie Nicolas[b], Nicolas Goudin[c], Meriem Garfa-Traore[c], Anita Fehér[d], Andras Dinnyés[d], Julien Nicolas[a], Patrick Couvreur[a], Simona Mura[a,*]

[a] *Institut Galien Paris-Sud, UMR 8612, CNRS, Univ Paris-Sud, Université Paris-Saclay, Faculté de Pharmacie, 5 rue Jean-Baptiste Clément, F-92296 Châtenay-Malabry cedex, France*

[b] *Institut Paris-Saclay d'Innovation Thérapeutique (IPSIT), UMS IPSIT Université Paris-Sud US 31 INSERM, UMS 3679 CNRS, Microscopy Facility, 5 rue Jean-Baptiste Clément, 92296 Châtenay-Malabry cedex, France*

[c] *Structure Fédérative de Recherche (SFR) Necker, Inserm US 24 CNRS UMS 3633, Cell Imaging Platform UMS 24, Hôpital Necker Enfants Malades, Bâtiment Imagine, 24 boulevard du Montparnasse, 75015 Paris, France*

[d] *BioTalentum Ltd, Aulich Lajos str. 26, 2100 Gödöllő, Hungary*

ARTICLE INFO

Keywords:
Multicellular tumor spheroids
Light sheet fluorescence microscopy
Confocal laser scanning microscopy
Drug penetration
Multi-view image fusion
3D tomography

ABSTRACT

We recently constructed a multicellular spheroid model of pancreatic tumor based on a triple co-culture of cancer cells, fibroblasts and endothelial cells and characterized by the presence of fibronectin, an important component of the tumor extracellular matrix. By combining cancer cells and stromal components, this model recreates *in vitro* the three-dimensional (3D) architecture of solid tumors. In this study, we used these hetero-type spheroids as a tool to assess the penetration of doxorubicin (used as a model drug) through the whole tumor mass either in a free form or loaded into polymer nanoparticles (NPs), and we investigated whether microscopy images, acquired by Confocal Laser Scanning Microscopy (CLSM) and Light Sheet Fluorescence Microscopy (LSFM), would be best to provide reliable information on this process. Results clearly demonstrated that CLSM was not suitable to accurately monitor the diffusion of small molecules such as the doxorubicin. Indeed, it only allowed to scan a layer of 100 μm depth and no information on deeper layers could be available because of a progressive loss of the fluorescence signal. On the contrary, a complete 3D tomography of the hetero-type multicellular tumor spheroids (MCTS) was obtained by LSFM and multi-view image fusion which revealed that the fluorescent molecule was able to reach the core of spheroids as large as 1 mm in diameter. However, no doxorubicin-loaded polymer nanoparticles were detected in the spheroids, highlighting the challenge of nanomedicine delivery through biological barriers. Overall, the combination of hetero-type MCTS and LSFM allowed to carry out a highly informative microscopic assessment and represents a suitable approach to precisely follow up the drug penetration in tumors. Accordingly, it could provide useful support in the preclinical investigation and optimization of nanoscale systems for drug delivery to solid tumors.

1. Introduction

An efficient chemotherapeutic treatment relies on the capacity of drugs, either in free form or loaded in nanoscale systems (*i.e.*, nanomedicines), to move through the tumor tissue and reach the target cells [1]. However, the complex physiopathology of solid tumors makes the penetration not straightforward. It is well known that the uncontrolled growth of cancer cells generates a solid pressure able to compress and obstruct blood and lymphatic vessels [2] and that this aberrant vasculature strongly limits cancer cell accessibility to nutrients, oxygen and also reduces their exposure to drugs [3]. If intravenous injected drugs/nanomedicines succeed to extravasate, the high interstitial fluid pressure and the thick extracellular matrix (ECM) would further hamper their path to the target cells. Consequently, they often accumulate in

* Corresponding author.
E-mail address: simona.mura@u-psud.fr (S. Mura).
[1] D.V. and A.B. contributed equally to this work.

https://doi.org/10.1016/j.ejpb.2019.06.019
Received 18 March 2019; Received in revised form 23 May 2019; Accepted 17 June 2019
Available online 20 June 2019

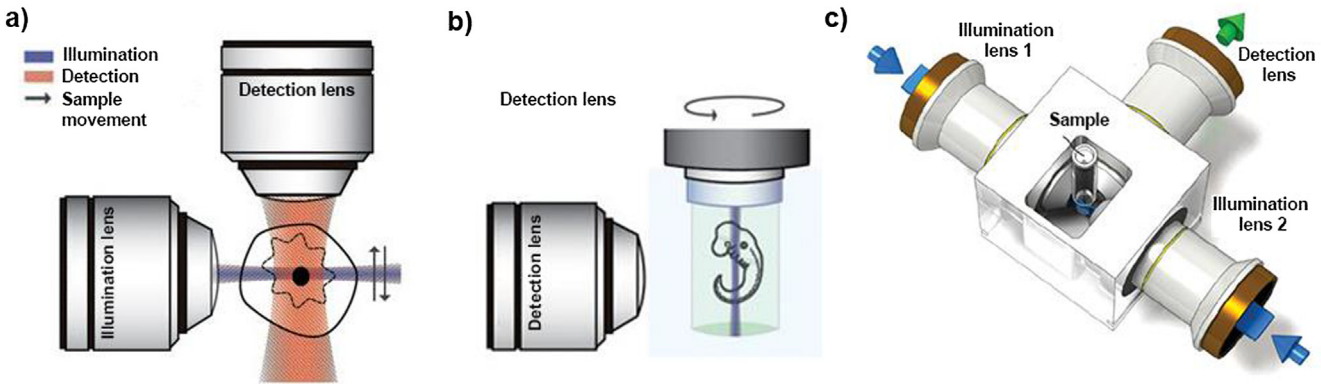

Fig. 1. Schematic illustration of (a) the LSFM detection and illuminations lenses (single illumination), (b) the mounting of a gel embedded-sample that allows the physical rotation for the multi-view imaging and (c) the LSFM in the dual-sided illumination configuration. Adapted with permission from ref. [41] and [39]. Copyright 2014 Springer Nature and 2012 Wiley Periodicals.

the perivascular space only [4,5] and the drug concentration in the tumor does not reach the optimal therapeutic level [6,7].

Although nanomedicines can improve the drug pharmacokinetics and reduce side effects caused by a nonspecific systemic distribution, they frequently suffer from the difficulty to efficiently cross the tumor biological barriers [8–10]. It has been demonstrated that different physicochemical properties strongly influence the penetration of drug delivery systems into the tumor mass and various strategies have been proposed to maximize their performances [11–13]. However, the predictive *in vitro* assessment of the capacity of tissue penetration still represents one of the main difficulties in the preclinical screening of any new nanomedicine [6]. It is evident that such information cannot arise from 2D cell cultures. Indeed, in conventional uptake studies, drugs and nanomedicines are added on the top of cancer cells grown on flat monolayers and the only barrier they must cross to reach the intracellular compartment is the cell membrane. Useful data can instead be collected using 3D cell culture models which are more representative of the biological reality as they reproduce *in vitro* the tumor and its microenvironment. Among them, multicellular tumor spheroids (MCTS) have attracted a great deal of attention thanks to their capacity to mimic key features of non-vascularized tumors such as the close contact among cells and their self-organization in layers with different proliferation rates [14,15]. In addition, cells in spheroids secrete ECM proteins thus allowing to recreate a microenvironment that acts as a biological barrier able to interfere with the transport phenomena and to block the diffusion of drugs and NPs [11,16].

However, the thickness of such 3D models represents a technical challenge making quite difficult the qualitative and quantitative *in vitro* assessment of the penetration of fluorescent drugs and NPs [17]. In order to overcome these issues, the penetration is often evaluated on spheroid slices sectioned at different depths from paraffin-embedded or frozen samples which are then imaged by conventional fluorescence microscopy [18–20]. However, spheroid sectioning is laborious and time consuming [21]. Moreover, although this strategy allows to obtain high quality images, it does not give a representative reconstruction of complex and heterogeneous 3D structures [22]. Alternatively, the penetration of fluorescent molecules into MCTS is largely assessed by Confocal Laser Scanning Microscopy (CLSM) through a virtual stack of optical sections [23–27]. In a CLSM set-up, the same lens is used for the excitation of the dyes and the detection of the emitted signals and the pinhole system allows to remove the out-of-focus light making possible the optical sectioning of the 3D samples [28]. However, the image resolution is generally restricted to depth distances of 60–80 μm [23,25,27] because both the excitation and emission lights, passing through the spheroid perpendicularly to the image plane, encounter a pronounced scattering [29]. The different refractive indices (Tyndall effect) and the non-uniform distribution of cells and extracellular components in the tissue cause wavelength-dependent phenomena of light scattering and absorption that degrade the quality of the fluorescence signals [30]. As a consequence, the number of emitted photons able to arise from the scanned sample decays exponentially with the increasing depth [31]. This problem could be partially solved by the use of higher wavelengths with two- or multi-photons microscopies [32–34]. However, because of the exposition of the whole sample to the excitation light during the imaging of each optical section, the above described techniques suffer in general from the production of important photobleaching and phototoxic effects. To be noted that in the case of the two /multi-photon microscopy the phenomenon is restricted to the focal plane in which excitation occurs [35].

In this context, the Light Sheet Fluorescence Microscopy (LSFM) has recently emerged as a suitable technique for the imaging of large biological specimens with high scattering properties [22,36–39]. This approach overcomes the limitations of traditional microscopies and allows deep sample scan at high imaging speed with minimal photodamage [28,36]. An illumination system (made of one or two illumination lenses) creates a light sheet of few microns thickness that scans the sample and excites only the fluorophores in the focused plane [40]. Since the detection lens is placed perpendicularly to the light sheet, the out-of-focus light is strongly reduced allowing a better definition of the scanned section (Fig. 1a) [29,41]. Thanks to the separation of illumination and detection pathways, only the detection objective is responsible for the lateral resolution [29,42]. The optical sectioning of large samples is then easily obtained by moving them through the focal plane. This translation along the optical axis of the detector creates a z-stack of images that can be used for the 3D reconstruction [43,44]. In recent years, the LSFM in combination with 3D models has been widely used in preclinical drug discovery to study morphological changes and toxic effects at the cellular level [17,30,44–47] and only few studies have proposed the use of this methodology to evaluate the penetration of drugs in simple spheroids made of only one cell type [48,49]. Whether such approach would be suitable also in systems with higher complexity remains a matter of question.

In this study we investigated the performance of these imaging methodologies to assess the penetration of doxorubicin (Dox) and Dox-loaded polymer NPs into a hetero-type MCTS model of pancreatic cancer recently developed in our team [50]. This model integrates both the cancerous component of the pancreatic tumor (cancer cells) and cellular/acellular components of the microenvironment (*that is,* fibroblasts, endothelial cells and extracellular matrix) and therefore represents a valuable model capable to mimic the obstacles to diffusion. The advantages of the LSFM compared to the traditional CLSM in terms of deep imaging and isotropic resolution were largely confirmed. Overall, the results collected from the multi-view imaging (Fig. 1b) provide a powerful example of the LSFM application *in vitro* on complex

hetero-type MCTS and strongly encourage its use since the earliest phases of preclinical screening of nanomedicines for tumor treatment.

2. Materials and methods

2.1. Cell lines

Human pancreatic cancer cells (PANC–1, ATCC, France) were maintained in Dulbecco's Modified Eagle Medium–high glucose (DMEM, Sigma Aldrich, France) supplemented with 10% heat-inactivated fetal bovine serum (FBS, Gibco, France). Human lung fibroblasts (MRC–5, ATCC, France) were cultured in Eagle's Minimum Essential Medium (EMEM, Sigma Aldrich, France) supplemented with 10% heat-inactivated FBS and 1% of 200 mM L-Glutamine solution (Sigma Aldrich, France). Human umbilical vein endothelial cells (HUVEC, ATCC, France) were maintained in endothelial growth medium (EGM–2) consisting of endothelial basal medium (EBM-2) in which supplements and growth factors were added according to manufacturer instruction (EGM-2 BulletKit Lonza, France). Cells were held in an incubator with a humid atmosphere at 37 °C with 5% CO_2, used below passage 8 after thawing and harvested at a confluence of 70–80%.

2.2. MCTS formation

Hetero-type MCTS containing pancreatic cancer cells, fibroblasts and endothelial cells were constructed according to the liquid overlay technique [51] in poly(-2-hydroxyethyl methacrylate) (PHEMA)-coated (1.2% (w/v)) 96-well round-bottom plates (CELLSTAR®, Sigma Aldrich, France).

A seeding ratio of 1:9:4 among PANC-1:MRC-5:HUVEC was used for the construction of both small (500:4500:2000 cells *per* well) and large (5000:45000:20000 cells *per* well) spheroids. As previously described [50], a fibronectin-gelatin nanometer-sized film was created at the MRC-5 surface before seeding according to the layer-by-layer method [52]. Briefly, after trypsinization, fibroblasts were suspended in 1 mL of Tris-HCl buffer (50 mM, pH 7.4) (Sigma Aldrich, France), centrifuged (2500 rpm, 1 min, room temperature) and then alternatively incubated for 1 min using a microtube rotator (VWR, France) in 1 mL of 0.04 $mg.mL^{-1}$ Human fibronectin or gelatin (Sigma Aldrich, France) Tris-HCl solutions (50 mM, pH 7.4). Each incubation was followed by a centrifugation (2500 rpm, 1 min, room temperature) and a washing step with Tris-HCl buffer (1 mL, 50 mM, pH 7.4). A total of 9 coating steps were performed. Then, fibroblasts were suspended in cell culture medium and used to construct the triple co-culture. Suspensions of each cell type (*that is*, PANC-1 cells, coated-MRC-5 and HUVEC) were prepared in DMEM complete medium supplemented with Human vascular endothelial growth factor (VEGF, 50 $ng.mL^{-1}$) (Thermo Fisher Scientific, France) and then 200 µL of their opportune mixture was transferred into each well. Automatic cell counting (Countess II, Thermo Fisher Scientific, France) was performed according to manufacturer instructions. After cell seeding, plates were centrifuged (1100 rpm, 5 min, 20 °C) and then incubated in a humidified atmosphere with 5% CO_2 at 37 °C for 4 days.

2.3. Optical imaging and spheroid volume measurement

Optical images were acquired using the AxioObserver Z1/Colibri/TIRF (Carl Zeiss, Germany) inverted microscope equipped with a Peltier cooled (−40 °C) CoolSnap HQ2 CCD camera (Photometrics, Tucson, USA) and an XL incubator thermostated at 37 °C providing 5% CO_2. By using a halogen lamp and a motorized stage in automated mode (ZenBlue software/high content acquisitions), transmitted light images of spheroids were collected directly from the PHEMA-coated plates with an EC Plan-Neofluar 2.5x/NA 0.085 dry objective lens.

Through an image-processing macro, specifically created with the Image-J® software, the minimum and major diameters of 40 spheroids were measured. Spheroid volume (V) was calculated according to the formula $V = [(a^2) * (b)]/2$, in which a and b represent the minor and major diameter, respectively.

2.4. Doxorubicin-loaded nanoparticles preparation and characterization

The drug-initiated method was used to grow a polyisoprene (PI) chain from a gemcitabine (Gem)-bearing initiator [53,54]. Then, a nitroxide exchange reaction was applied to post-functionalize the polymer with doxorubicin (Dox) [55–57]. In this way, a Gem-PI-Dox heterotelechelic (dual functionalized) polymer prodrug was synthesized (Fig. 7) [57]. Nanoparticles were formulated according to the nanoprecipitation metod [58]. In brief, 2.5 mg of the polymer were dissolved in 0.5 mL of tetrahydrofuran and quickly added to 1 mL of MilliQ water. The organic solvent was then evaporated at room temperature under vacuum (Buchi Rotavapor, France). The nanoparticle diameter was measured by dynamic light scattering (DLS) with a Nano ZS from Malvern (173° scattering angle) at a temperature of 25 °C after 1:20 dilution in MilliQ water. The surface charge of the nanoparticles was investigated by zeta potential (mV) measurement at 25 °C after a 1:10 dilution with 1 mM NaCl by applying the Smoluchowski equation and using the same instrument. The morphology of the nanoparticles was observed by Transmission Electron Microscopy (TEM) using a JEOL JEM-1400 microscope operating at 80 kV. Images were acquired using an Orius camera (Gatan Inc, USA). 5 µL of diluted nanoparticle suspension (0.1%, v/v) were deposited for 30 s on glow-discharged copper grids covered with formvar-carbon film. The excess solution was blotted off using a filter paper. Samples were then immersed for 5 min in a drop of uranyl acetate solution (2 wt%) for negative staining.

2.5. 3D spheroid penetration assessment with CLSM

Small hetero-type MCTS (500:4500:2000 cells *per* well) were prepared and cultured for 4 days before incubation with doxorubicin at a concentration of 20 µM in culture medium. After 3 h of incubation at 37 °C, MCTS were harvested, transferred in a microtube and then the culture medium was carefully removed. Spheroids were washed once with 200 µL of phosphate buffered saline (PBS, Sigma Aldrich, France) and fixed in 500 µL of 4% paraformaldehyde (Roti®-Histofix 4%) (1 h, room temperature). Samples were imaged with an inverted Confocal Laser Scanning Microscope (LSM 510-Meta, Carl Zeiss, Germany) using a dry Plan-Apochromat 20x/NA0.75 objective lens, equipped with an argon laser (488 nm excitation wavelength). The red fluorescence emission was collected with a 560 nm long pass (LP) emission filter. The pinhole was set at 1.0 Airy unit. 12-bit numerical images were acquired with the LSM 510 software version 3.2.

2.6. 3D spheroid penetration assessment with LSFM

Small (500:4500:2000 cells *per* well) and large (5000:45000:20000 cells *per* well) hetero-type MCTS were prepared and cultured for 4 days before incubation with Dox or Dox-loaded NPs (20 µM in culture medium). Small and large MCTS were harvested after 3 h and 4 h of incubation at 37 °C, respectively. The culture medium was carefully removed and, after one washing step in PBS (200 µL), spheroids were fixed in 500 µL of 4% paraformaldehyde (Roti®-Histofix 4%) (1 h, room temperature). To facilitate the post-imaging z-stack fusion, nuclei of large MCTS were stained. Thus, after fixation, MCTS were permeabilized with 500 µL of 0.1% Triton X-100 (Sigma Aldrich, France) in PBS (1 h, room temperature). Then, the Triton solution was replaced with 200 µL of PBS and spheroids were stained at least for 24 h with Hoechst 33342 (NucBlue™ Reagent, Thermo Fisher Scientific, France) in the dark at room temperature. Spheroids were then kept in the dark with the nuclei staining solution until imaging. To perform the LSFM imaging, samples (small and large MCTS) were embedded in 0.8% low-

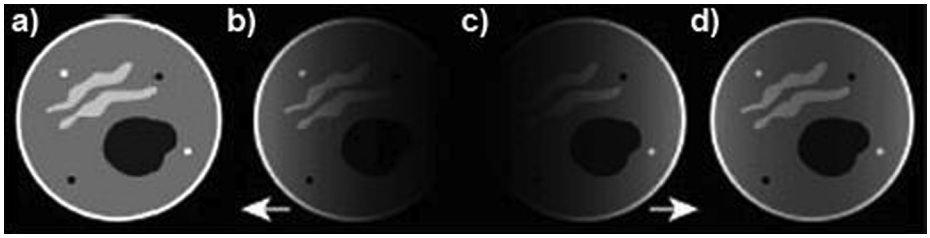

Fig. 2. Schematic representation of image distortion due to the spatial modification of the quality of the image and the compensation obtained by multi-view imaging and z-stack fusion. (a) Original non distorted image; (b) z-stack collected with detection at 0° (from the left); (c) z-stack collected with detection at 180° (from the right); (d) optical fusion of (b) and (c) in a single data set with better spatial resolution. Arrows indicate the axis along which the light is detected. Adapted with permission from ref. [59]. Copyright 2007 OSA Publishing.

melting agarose (Thermo Fisher Scientific, France) by using a glass cylindrical capillary and then images were acquired with a Lightsheet Z.1 Microscope (Carl Zeiss, Germany) equipped with a Plan-Apochromat 20x/NA1 water-immersion objective lens with left and right illumination. Red (doxorubicin) and blue (Hoechst) fluorescence signals were recorded after sample excitation at 488 and 405 nm, respectively. Samples were scanned using the Zen 2014 SP1 Black-Edition software (Carl Zeiss, Germany) with a 575–615 nm band pass (BP) emission filter for Dox and a 420–470 nm BP emission filter for Hoechst. For small spheroids, collected optical slices were processed for the 3D reconstruction by maximum intensity projection (MIP) with the ImageJ® software. With the large MCTS, a 3D tomography was obtained with the Imaris Stitcher® software (Bitplane AG, Zurich - Switzerland) by fusion of two z-stacks collected from two independent views of the same sample (0° and 180°). This approach allowed to make up for the low quality of the images acquired in the deepest part of the sample and permitted to collect relevant information from the different regions (Fig. 2). The Imaris® software (Bitplane AG, Zurich - Switzerland) was used to render the 3D representation of the entire spheroid and select single optical sections.

2.7. 2D cellular uptake assessment with CLSM

Twelve-mm diameter confocal microscopy round coverslips (Thermo Fisher Scientific, France) were placed on a 24-well plate. PANC-1 cells were seeded at a density of 1.5×10^5 cells *per* well in complete medium. Cells were cultured for 24 h and then the medium was discarded and replaced with 300 µL of free Dox or Dox-loaded NPs in complete medium at a concentration of 10 µM. After 90 min of incubation at 37 °C, cells were gently washed once with 300 µL of PBS and fixed by 20 min treatment with 4% paraformaldehyde. Then, the cell nuclei were stained by 20 min treatment with 200 µL of Hoechst 33342 solution in PBS. Finally, cells were washed twice with 300 µL of PBS and covered with a coverglass by using Vectashield® (Vector Laboratories, USA) as mounting medium. Samples were imaged with an inverted Confocal Laser Scanning Microscope TCS SP8 (Leica, Germany) using a CS2 Plan Apochromat 63x/NA 1.4 oil immersion objective lens. The instrument was equipped with a WLL Laser (488 nm) and a 405 nm diode for Dox and Hoechst 33342 excitation, respectively. The red fluorescence emission was collected with a 558–708 nm wide emission slits and the blue fluorescence emission was collected with a 412–466 nm wide emission slits. Transmission images were acquired with the 488 nm laser line and a PMT-trans detector. The pinhole was set at 1.0 Airy unit. 12-bit numerical images were made with the Leica SP8 LAS X software (Version 3.1.5; Leica, Germany).

3. Results and discussion

3.1. Penetration studies with CLSM

Pancreatic tumor spheroids made of cancer cells and stromal components were constructed by seeding 500 PANC-1 cancer cells, 4500 MRC-5 fibroblasts and 2000 HUVEC cells *per* well (1:9:4 ratio) in non-adherent PHEMA–coated 96-well round-bottom plates. As previously described, a 3D model integrating the three cellular components and capable to mimic the heterogeneity of the pancreatic tumor was obtained after 4 days of culture. At this time point, spheroids showed an average diameter of about 600 µm [50].

Herein, we used this model to investigate the drug penetration by incubating spheroids with doxorubicin, an anticancer drug showing high DNA affinity [60] and fluorescence properties useful for *in vitro* imaging [6]. After 3 h of incubation, the penetration of Dox was firstly assessed by Confocal Laser Scanning Microscopy using a z-stack of 149 focal planes and a step pass of 0.98 µm. Virtual slices were recorded until complete loss of the fluorescence signal and subsequently rendered as a maximum intensity projection (MIP) for the 3D reconstruction (Fig. 3a). The total scanned portion was approximately of 145 µm. The MIP clearly showed doxorubicin intercalation in DNA, which resulted in a strong red fluorescence in all cell nuclei at the spheroid surface. However, the MIP did not provide any information about the depth of penetration, whose appreciation required the analysis of single optical sections from the z-stack. The optical section taken at ~5 µm depth, showed Dox internalization and accumulation in the nuclei of cells of the external layer of the spheroid, which appeared quite rough and somehow irregular (Fig. 3b). Dox penetration could be observed up to 50 µm depth, even if a slight decrease of fluorescence was already noticed (Fig. 3c). Then, the continuous loss of Dox fluorescence in the deepest layers strongly reduced the imaging quality of the spheroid core and at a distance of about 100 µm from the spheroid surface (Fig. 3d), the real degree of drug penetration could not be estimated. The absence of signal in the inner part of the spheroid was to ascribe to either: *(i)* the absence of doxorubicin (*that is*, the drug was unable to reach this area)

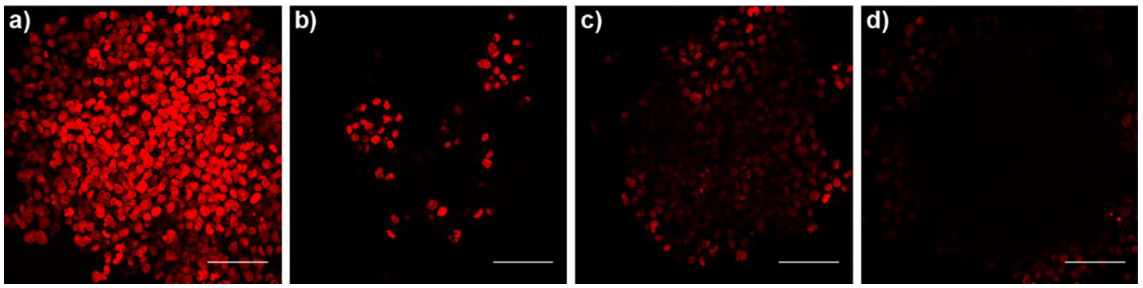

Fig. 3. Confocal imaging of MCTS after incubation with doxorubicin (20 µM) for 3 h at 37 °C. (a) Maximum intensity projection (MIP) of the z-stack; (b) optical section n° 5 at ~5 µm depth; (c) optical section n° 50 at ~50 µm depth and (d) optical section n° 100 at ~100 µm depth. Scale bars: 100 µm.

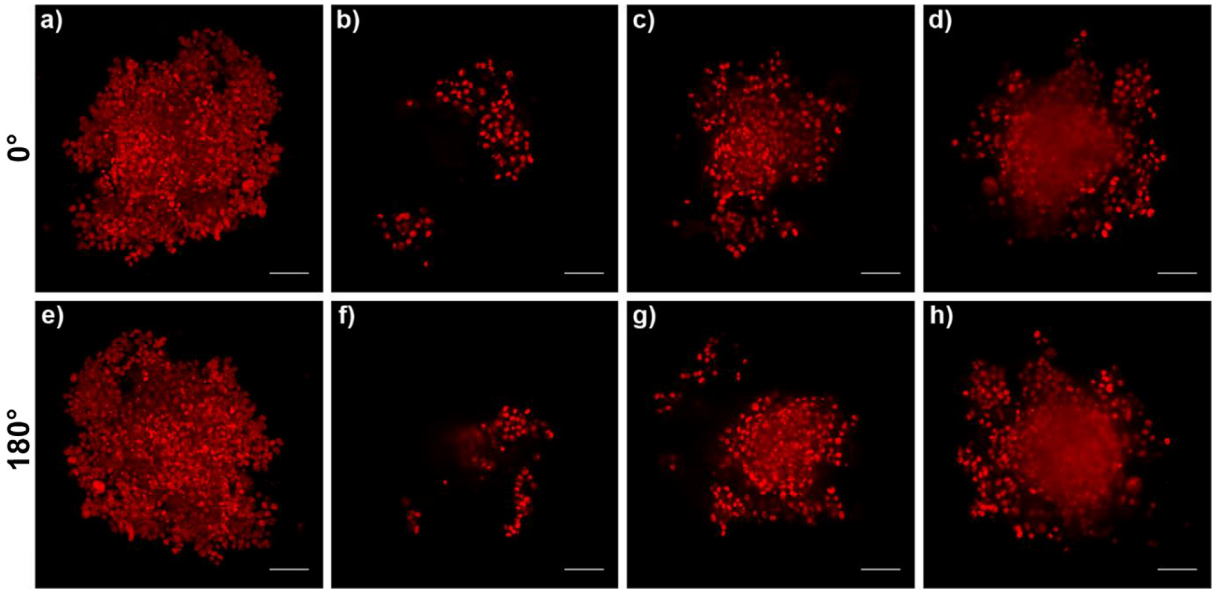

Fig. 4. LSFM imaging of MCTS after incubation with doxorubicin (20 μM, 3 h, 37 °C). Images from the z-stack recorded at 0°: (a) maximum intensity projection (MIP); (b) optical section n° 80 at ~58 μm depth; (c) optical section n° 150 at ~110 μm depth and (d) optical section from the middle (n° 260) at ~190 μm depth. Images from the z-stack recorded after 180° rotation of the sample: (e) maximum intensity projection (MIP); (f) optical section n° 80 at ~58 μm depth; (g) optical section n° 150 at ~110 μm depth and (h) optical section from the middle (n° 267) at ~195 μm depth. Scale bars: 100 μm.

or *(ii)* the scattering and absorption of the 3D tissue. These hypotheses could not be verified by CLSM, thus clearly demonstrating the limitation of this imaging technique in the investigation of drug diffusion into spheroids.

3.2. Penetration studies with LSFM

Can doxorubicin penetrate through these spheroids entirely until their core? An unequivocal answer to this question could not be obtained by CLSM. Thus, hetero-type MCTS incubated with doxorubicin following the same experimental set up (*i.e.*, concentration of 20 μM, 3 h) were imaged with the Carl Zeiss Lightsheet Z.1 microscope. This Selective Plane Illumination Microscope (SPIM) was equipped with two lenses for a double-sided illumination of the sample (Fig. 1c) and a light-sheet pivoting system able to create a regular exposition and to reduce stripe artefacts [41,61]. The spheroid was embedded in an agarose column by filling a glass capillary connected to a motor that allowed the physical rotation of the sample (Fig. 1b) for the acquisition of z-stacks from different rotation angles [30,62]. The MIP of the whole spheroid (observation angle 0°) was reconstructed from 521 optical sections recorded every 0.73 μm. This projection (Fig. 4a), which confirmed the results obtained by CLSM (Fig. 3a), also clearly demonstrated the capacity of doxorubicin to penetrate into the cells and then reach the nuclei. While CLSM failed to assess the drug penetration in the deeper layers, herein the analysis of single planes highlighted the higher performance of LSFM. Indeed, the light sheet allowed to scan the spheroid from the surface to the core without loss of the fluorescence signal (Fig. 4b-d). Also, the collected images showed that the drug was able to diffuse uniformly in the peripheral layers (Fig. 4b) as well as in the inner ones (Fig. 4d). Once arrived in the centre, the spheroid was turned by 180° to also image, with high resolution, the other half of the sample. Such multi-view imaging is a specific feature of the LSFM and, interestingly, it requires only a short acquisition time thanks to the employment of a Charge-Coupled Device (CCD) camera [41,59]. 535 other optical sections with a step pass of 0.73 μm were collected and allowed to definitively demonstrate the presence of a fluorescence signal in the whole spheroid and confirmed that doxorubicin was capable to diffuse through the entire sample (Fig. 4e–h). Overcoming the limited isotropic resolution of the conventional confocal technique, LSFM permitted a highly informative imaging, thus clarifying the non-conclusive results obtained by CLSM.

To further prove the potential of the LSFM technique, we applied it to the imaging of larger spheroids, which in addition offered the opportunity to test the 3D tomography as post-imaging reconstruction [59,63] through the fusion of two z-stacks independently recorded at 0° and 180°.

Hetero-type MCTS with a diameter of ~1 mm were constructed by keeping constant the cell ratio (1:9:4, PANC-1:MRC-5:HUVEC) but increasing 10 times the cell number (Fig. 5).

Following spheroid incubation with doxorubicin (20 μM, 4 h), the cell nuclei were stained with Hoechst 33342 which allowed to display the whole 3D mass during the acquisition and facilitated the merging of the z-stacks during the processing. Problems related to light scattering and absorption are frequent with such large specimens [38,44]. Thus, images from the different optical planes were collected until the first shadowing of the blue fluorescence signal occurred. Then, the sample rotation of 180° and the acquisition of the second z-stack ensured the imaging of the whole spheroid. The final fusion of the two z-stacks generated a single data set of 324 focal planes spaced of 2.90 μm along

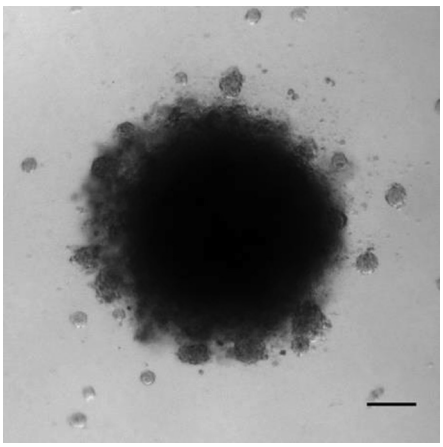

Fig. 5. Representative optical image of large MCTS (5000 PANC-1 + 45000 MRC-5 + 20000 HUVEC cells/well) at day 4 post seeding. Scale bar: 200 μm.

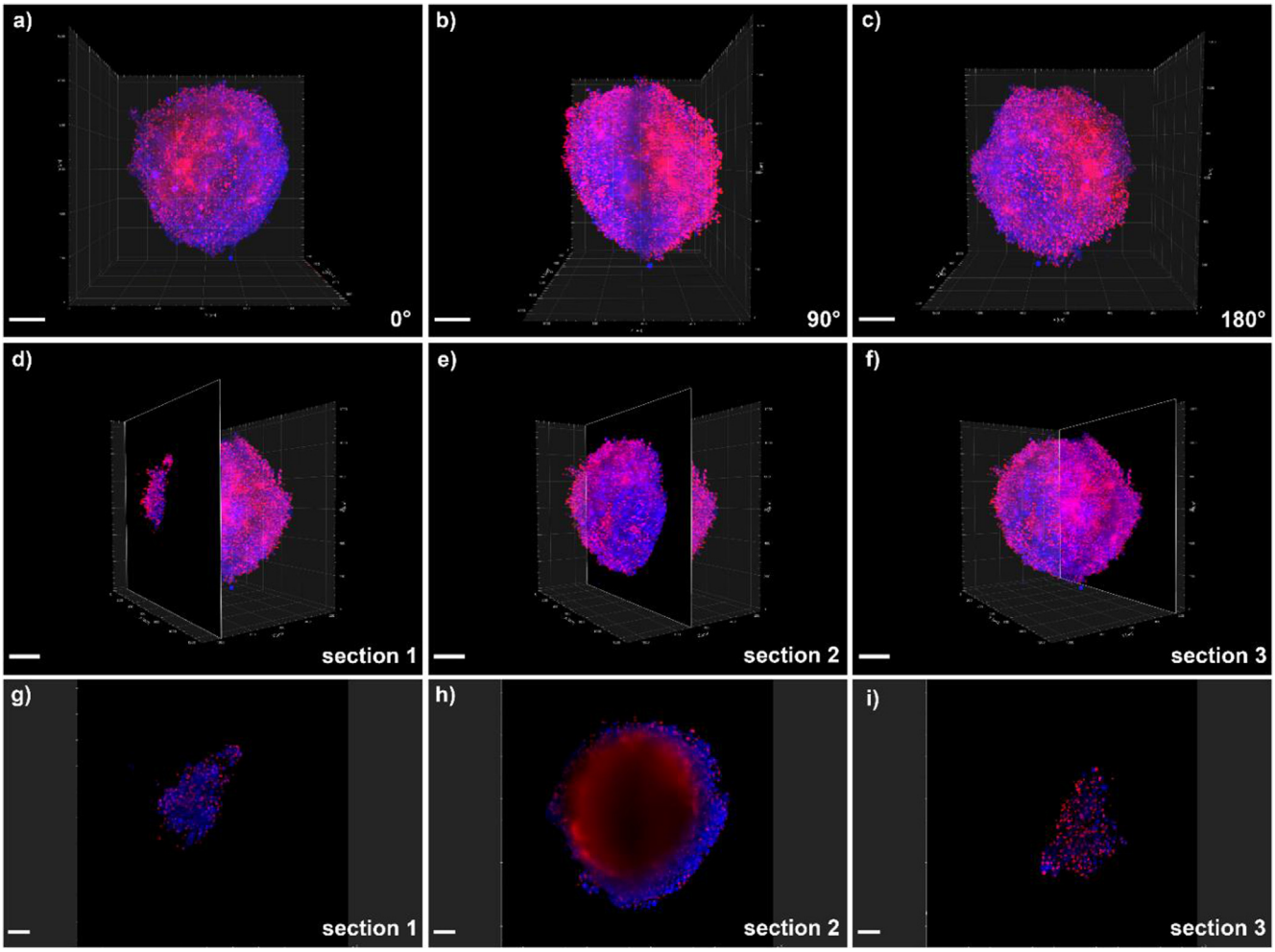

Fig. 6. 3D tomography with LSFM of large MCTS after incubation with 20 μM of Dox for 4 h at 37 °C. Overlays of blue (nuclei, Hoechst 33342 staining) and red (Dox) channels. (a) 0° rotation; (b) 90° rotation and (c) 180° rotation. Localization of (d) section 1 (~113 μm depth); (e) section 2 (~403 μm depth) and (f) section 3 (~861 μm depth) in relation to the entire spheroid. Scale bars: 200 μm. Images taken at (g) section 1; (h) section 2 and (i) section 3. Scale bars: 100 μm. (For interpretation of the references to colour in this figure legend, the reader is referred to the web version of this article.)

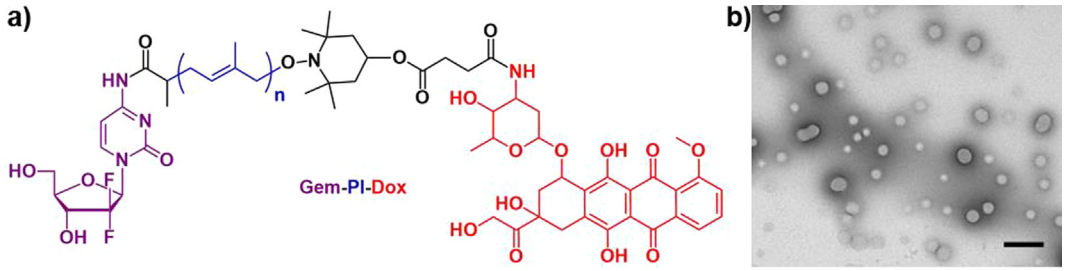

Fig. 7. (a) Structure of heterobifunctional gemcitabine-polyisoprene-doxorubicin (Gem-PI-Dox) polymer prodrug; (b) representative TEM image of Gem-PI-Dox nanoparticles. Scale bar: 1 μm.

the z-axis. Their 3D complete reconstruction enabled to assess the spherical volume of the sample in which the red fluorescence of the drug matched with all visible cell nuclei (Fig. 6a–c). The doxorubicin penetration in the whole spheroid was demonstrated by three different optical sections, recorded at depths of 113, 403 and 861 μm (Fig. 6d–i). To be noted that section 2 was obtained from the middle of the sample and evidenced the ability of doxorubicin to diffuse deeply and reach the core of the spheroid (Fig. 6e, h). The red fluorescence signal was visible in the central part of the sample though the signal was shadowed and hindered the clear distinction of the doxorubicin in the nuclei as consequence of strong scattering phenomena.

Overall these results confirmed the penetration capacity of small molecules into large spheroids and data were in agreement with the penetration depth demonstrated by other advanced microscopic systems [16,49].

In the last decades, nanoscale drug delivery systems have been proposed to overcome the limitations associated with the administration of free drugs (*e.g.*, rapid drug metabolization, excretion, non-specific cell or tissue biodistribution and insurgence of resistance phenomena). Interestingly enough, doxorubicin has also been loaded into various nanoparticulate systems such as liposomes, polymer nanoparticles or micelles [64–68]. In this context, our group, which has been working on the formulation of polymer prodrug nanoparticles since several years, recently developed innovative heterotelechelic polymer

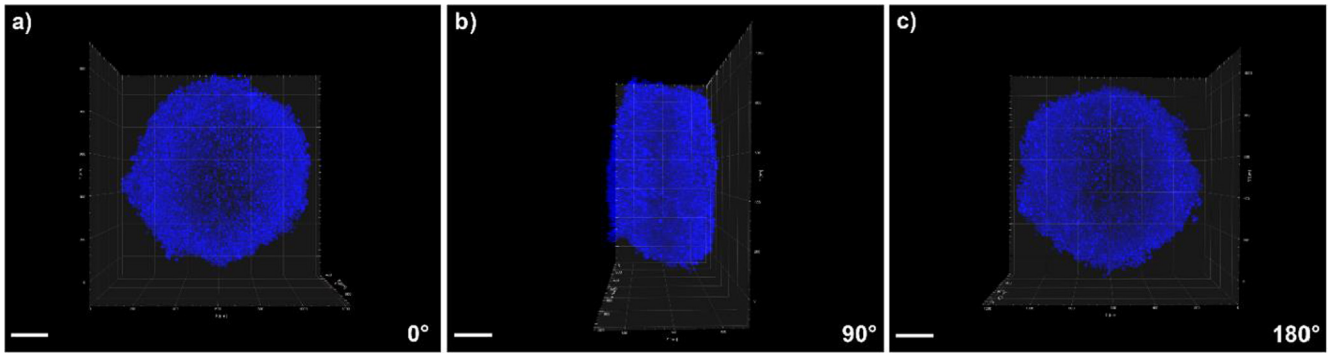

Fig. 8. 3D tomography with LSFM of large MCTS after incubation with Dox-loaded NPs (20 μM equiv. Dox, 4 h, 37 °C). Overlays of blue (nuclei, Hoechst 33342 staining) and red (Dox) channels. (a) 0° rotation; (b) 90° rotation and (c) 180° rotation. Scale bars: 200 μm. (For interpretation of the references to colour in this figure legend, the reader is referred to the web version of this article.)

prodrugs comprising two different anticancer drugs (*e.g.,* doxorubicin and gemcitabine) linked at the extremity [57]. By simple nanoprecipitation of an organic solution of these polymer prodrugs in water, spherical nanoparticles, with a mean diameter of ca. 100 nm, narrow size distribution, and negative surface charge (−25 mV) were obtained (Fig. 7).

Taking advantage of the fluorescence properties of doxorubicin, we have investigated the ability of these NPs to diffuse through the tumor mass. The NP penetration was investigated following incubation (20 μM equiv. doxorubicin, 4 h) with large spheroids. Spheroids were then imaged by SPIM and 295 optical sections from the entire spheroid were collected and merged. Images were recorded every 2.90 μm by two independent z-stacks at 0° and 180°. Opposite to what was observed with the free drug no red fluorescence signal was detectable after 4 h of incubation (Fig. 8) suggesting that these Dox-loaded NPs might have inferior penetration ability into hetero-type spheroids. The fast penetration of free doxorubicin is likely the result of its rapid diffusion in the ECM and in the interstitial spaces between cells, before being internalized and avidly bound to DNA [6,60]. A similar behavior was likely hindered by the hydrophobic surface of the nanoparticles and their larger size, demonstrating the influence of the physico-chemical features on the diffusion capacity in this 3D tumor model harboring a dense ECM. This was in agreement with the previous observation of Kataoka and coworkers which showed that large micelles (100 nm diameter) hardly diffused in fibrosis-rich pancreatic tumors *in vivo* [69].

To be noted that, when these NPs were incubated with 2D monolayers of PANC-1 cancers cells, their cellular internalization was even observed at an earlier time point as shown by confocal microscopy (Fig. 9). However, the extent of uptake was quite poor and probably not enough to ensure significant penetration into the spheroid. Noteworthy is that, although low, this signal was detected by CLSM thanks to the larger numerical aperture compared to the LSFM.

Overall these data clearly confirm that a reliable prediction of the capacity of nanoparticles to reach the target cells and efficiently delivery their cargo requires the use of models capable to reproduce the complexity of the tumor tissue with multiple biological barriers. In addition, when moving to such models, opportune powerful imaging techniques are imperatively needed to strongly reduce the risk of artefactual interpretation of the experimental data, which is a situation that can happen when using confocal microcopy techniques only.

4. Conclusions

In this study we have shown that Light Sheet Fluorescence Microscopy, allowing to overcome the limitations of traditional confocal imaging techniques, offered the possibility to precisely discriminate the capacity of free doxorubicin and drug-loaded nanocarriers to penetrate (or not) in a complex 3D tumor model of pancreatic tumor. By sample imaging with a Selective Plane Illumination Microscope we, indeed, succeeded in monitoring the fluorescence signal in the whole spheroid without loss of resolution and, thanks to complete 3D tomography of the MCTS, we confirmed that doxorubicin was capable to reach the spheroid core. Moreover, we did not observe any penetration of nanoparticles in this stroma rich-model, while they have easily been visualized intracellularly when incubated with cancer cells cultured in 2D. The strength of the LSFM for the imaging of large sample is well known but our results stress on the fact that the increase in complexity of *in vitro* models must be accompanied by an increase of the appropriateness of the instruments used for their analysis. To our knowledge, the results herein presented show for the first time a comparison on the application of these two imaging modalities in the analysis of drug/nanomedicine penetration. And this

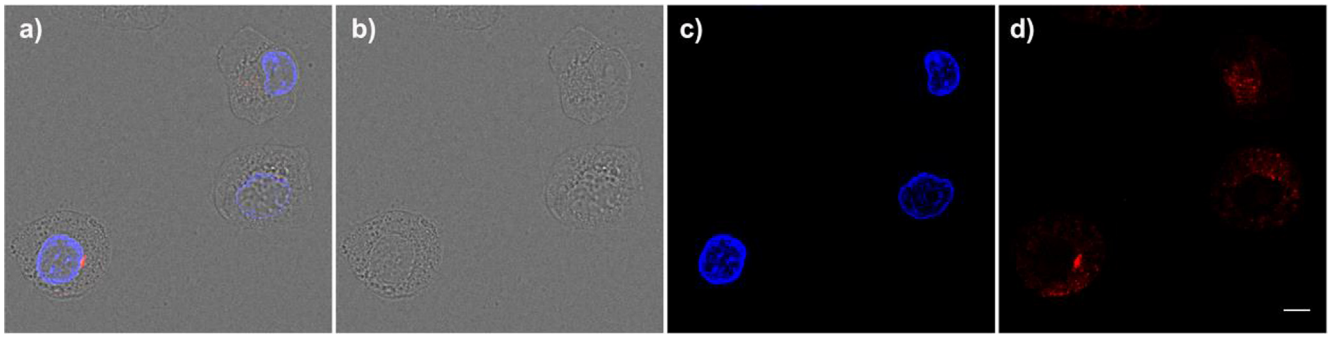

Fig. 9. Confocal imaging of PANC-1 monolayer (2D) after incubation with Dox-loaded NPs (10 μM equiv. Dox) for 90 min at 37 °C. (a) Overlay of brightfield, blue (Hoechst 33342, nuclei) and red (Dox-loaded NPs) channels; (b) brightfield image of PANC-1 cells; (c) single blue channel showing cell nuclei and (d) single red channel showing internalized Dox-loaded NPs. Scale bar: 10 μm. (For interpretation of the references to colour in this figure legend, the reader is referred to the web version of this article.)

should strongly encourage the use of opportune tools to carry out a reliable preclinical *in vitro* screening of nanomedicines.

Acknowledgements

The research leading these results has received funding from the European Union's Horizon 2020 research and innovation program under Marie Skłodowska Curie grant agreement no. 642028. The CNRS (Centre national de la recherche scientifique) and the French Ministry of Research are also warmly acknowledged for the financial support.

Declaration of Competing Interest

The authors declare no conflict of interest.

References

[1] I.F. Tannock, C.M. Lee, J.K. Tunggal, D.S.M. Cowan, M.J. Egorin, Limited penetration of anticancer drugs through tumor tissue, Clin. Cancer Res. 8 (3) (2002) 878.
[2] T.P. Padera, B.R. Stoll, J.B. Tooredman, D. Capen, E.D. Tomaso, R.K. Jain, Cancer cells compress intratumour vessels, Nature 427 (2004) 695.
[3] J.M. Brown, W.R. Wilson, Exploiting tumour hypoxia in cancer treatment, Nat. Rev. Cancer 4 (2004) 437.
[4] Y. Matsumoto, J.W. Nichols, K. Toh, T. Nomoto, H. Cabral, Y. Miura, R.J. Christie, N. Yamada, T. Ogura, M.R. Kano, Y. Matsumura, N. Nishiyama, T. Yamasoba, Y.H. Bae, K. Kataoka, Vascular bursts enhance permeability of tumour blood vessels and improve nanoparticle delivery, Nat. Nanotechnol. 11 (2016) 533.
[5] A.J. Primeau, A. Rendon, D. Hedley, L. Lilge, I.F. Tannock, The distribution of the anticancer drug doxorubicin in relation to blood vessels in solid tumors, Clin. Cancer Res. 11 (24) (2005) 8782.
[6] A.I. Minchinton, I.F. Tannock, Drug penetration in solid tumours, Nat. Rev. Cancer 6 (2006) 583.
[7] O. Trédan, C.M. Galmarini, K. Patel, I.F. Tannock, Drug resistance and the solid tumor microenvironment, J. Natl. Cancer Inst. 99 (19) (2007) 1441–1454.
[8] D.L. Stirland, J.W. Nichols, S. Miura, Y.H. Bae, Mind the gap: A survey of how cancer drug carriers are susceptible to the gap between research and practice, J. Control. Release 172 (3) (2013) 1045–1064.
[9] V.J. Venditto, F.C. Szoka, Cancer nanomedicines: so many papers and so few drugs!, Adv. Drug Deliv. Rev. 65 (1) (2013) 80–88.
[10] Y.-R. Zhang, R. Lin, H.-J. Li, W.-L. He, J.-Z. Du, J. Wang, Strategies to improve tumor penetration of nanomedicines through nanoparticle design, Wiley Interdiscip. Rev. Nanomed. Nanobiotechnol. 11 (1) (2019) e1519.
[11] G. Lazzari, P. Couvreur, S. Mura, Multicellular tumor spheroids: a relevant 3D model for the in vitro preclinical investigation of polymer nanomedicines, Polym. Chem. 8 (34) (2017) 4947–4969.
[12] Q. Sun, T. Ojha, F. Kiessling, T. Lammers, Y. Shi, Enhancing tumor penetration of nanomedicines, Biomacromolecules 18 (5) (2017) 1449–1459.
[13] I.-K. Choi, R. Strauss, M. Richter, C.-O. Yun, A. Lieber, Strategies to increase drug penetration in solid tumors, Front. Oncol. 3 (193) (2013).
[14] E.C. Costa, A.F. Moreira, D. de Melo-Diogo, V.M. Gaspar, M.P. Carvalho, I.J. Correia, 3D tumor spheroids: an overview on the tools and techniques used for their analysis, Biotechnol. Adv. 34 (8) (2016) 1427–1441.
[15] E. Fennema, N. Rivron, J. Rouwkema, C. van Blitterswijk, J. de Boer, Spheroid culture as a tool for creating 3D complex tissues, Trends Biotechnol. 31 (2) (2013) 108–115.
[16] H.L. Ma, Q. Jiang, S. Han, Y. Wu, T.J. Cui, D. Wang, Y. Gan, G. Zou, X.J. Liang, Multicellular tumor spheroids as an in vivo-like tumor model for three-dimensional imaging of chemotherapeutic and nano material cellular penetration, Mol. Imaging 11 (6) (2012) 487–498.
[17] F. Pampaloni, E.G. Reynaud, E.H.K. Stelzer, The third dimension bridges the gap between cell culture and live tissue, Nat. Rev. Mol. Cell Biol. 8 (2007) 839.
[18] H. Gao, Z. Yang, S. Zhang, S. Cao, Z. Pang, X. Yang, X. Jiang, Glioma-homing peptide with a cell-penetrating effect for targeting delivery with enhanced glioma localization, penetration and suppression of glioma growth, J. Control. Release 172 (3) (2013) 921–928.
[19] T.H. Kim, C.W. Mount, W.R. Gombotz, S.H. Pun, The delivery of doxorubicin to 3-D multicellular spheroids and tumors in a murine xenograft model using tumor-penetrating triblock polymeric micelles, Biomaterials 31 (28) (2010) 7386–7397.
[20] W. Ke, J. Li, K. Zhao, Z. Zha, Y. Han, Y. Wang, W. Yin, P. Zhang, Z. Ge, Modular design and facile synthesis of enzyme-responsive peptide-linked block copolymers for efficient delivery of doxorubicin, Biomacromolecules 17 (10) (2016) 3268–3276.
[21] P. Brandtzaeg, The increasing power of immunohistochemistry and immunocytochemistry, J. Immunol. Methods 216 (1) (1998) 49–67.
[22] I. Smyrek, E.H.K. Stelzer, Quantitative three-dimensional evaluation of immunofluorescence staining for large whole mount spheroids with light sheet microscopy, Biomed. Opt. Express 8 (2) (2017) 484–499.
[23] X. Jiang, H. Xin, J. Gu, X. Xu, W. Xia, S. Chen, Y. Xie, L. Chen, Y. Chen, X. Sha, X. Fang, Solid tumor penetration by integrin-mediated pegylated poly(trimethylene carbonate) nanoparticles loaded with paclitaxel, Biomaterials 34 (6) (2013) 1739–1746.
[24] C. Sarisozen, S. Dhokai, E.G. Tsikudo, E. Luther, I.M. Rachman, V.P. Torchilin, Nanomedicine based curcumin and doxorubicin combination treatment of glioblastoma with scFv-targeted micelles: In vitro evaluation on 2D and 3D tumor models, Eur. J. Pharm. Biopharm. 108 (2016) 54–67.
[25] G.L. Hu, Y. Wang, Q. He, H.L. Gao, Multistage drug delivery system based on microenvironment-responsive dendrimer–gelatin nanoparticles for deep tumor penetration, RSC Adv. 5 (104) (2015) 85933–85937.
[26] A.W. Du, H. Lu, M. Stenzel, Stabilization of paclitaxel-conjugated micelles by cross-linking with cystamine compromises the antitumor effects against two- and three-dimensional tumor cellular models, Mol. Pharmaceutics 13 (11) (2016) 3648–3656.
[27] R.I. Dmitriev, S.M. Borisov, H. Düssmann, S. Sun, B.J. Müller, J. Prehn, V.P. Baklaushev, I. Klimant, D.B. Papkovsky, Versatile conjugated polymer nanoparticles for high-resolution O_2 imaging in cells and 3D tissue models, ACS Nano 9 (5) (2015) 5275–5288.
[28] F. Pampaloni, N. Ansari, E.H.K. Stelzer, High-resolution deep imaging of live cellular spheroids with light-sheet-based fluorescence microscopy, Cell Tissue Res. 352 (1) (2013) 161–177.
[29] T. Bruns, S. Schickinger, R. Wittig, H. Schneckenburger, Preparation strategy and illumination of three-dimensional cell cultures in light sheet-based fluorescence microscopy, SPIE (2012) 5.
[30] A. Feuchtinger, A. Walch, M. Dobosz, Deep tissue imaging: a review from a preclinical cancer research perspective, Histochem. Cell Biol. 146 (6) (2016) 781–806.
[31] J. Andilla, R. Jorand, O.E. Olarte, A.C. Dufour, M. Cazales, Y.L.E. Montagner, R. Ceolato, N. Riviere, J.-C. Olivo-Marin, P. Loza-Alvarez, C. Lorenzo, Imaging tissue-mimic with light sheet microscopy: a comparative guideline, Sci. Rep. 7 (2017) 44939.
[32] F. Helmchen, W. Denk, Deep tissue two-photon microscopy, Nat Meth 2 (12) (2005) 932–940.
[33] J.S. Basuki, H.T.T. Duong, A. Macmillan, R.B. Erlich, L. Esser, M.C. Akerfeldt, R.M. Whan, M. Kavallaris, C. Boyer, T.P. Davis, Using fluorescence lifetime imaging microscopy to monitor theranostic nanoparticle uptake and intracellular doxorubicin release, ACS Nano 7 (11) (2013) 10175–10189.
[34] U. Till, L. Gibot, P. Vicendo, M.P. Rols, M. Gaucher, F. Violleau, A.F. Mingotaud, Crosslinked polymeric self-assemblies as an efficient strategy for photodynamic therapy on a 3D cell culture, RSC Adv. 6 (74) (2016) 69984–69998.
[35] A. Ustione, D.W. Piston, A simple introduction to multiphoton microscopy, J. Microsc. 243 (3) (2011) 221–226.
[36] P.J. Keller, A.D. Schmidt, J. Wittbrodt, E.H.K. Stelzer, Reconstruction of zebrafish early embryonic development by scanned light sheet microscopy, Science 322 (5904) (2008) 1065.
[37] P.J. Verveer, J. Swoger, F. Pampaloni, K. Greger, M. Marcello, E.H.K. Stelzer, High-resolution three-dimensional imaging of large specimens with light sheet–based microscopy, Nat. Meth. 4 (2007) 311.
[38] C. Lorenzo, C. Frongia, R. Jorand, J. Fehrenbach, P. Weiss, A. Maandhui, G. Gay, B. Ducommun, V. Lobjois, Live cell division dynamics monitoring in 3D large spheroid tumor models using light sheet microscopy, Cell Division 6 (1) (2011) 22.
[39] J. Huisken, Slicing embryos gently with laser light sheets, BioEssays 34 (5) (2012) 406–411.
[40] F. Pampaloni, B.-J. Chang, E.H.K. Stelzer, Light sheet-based fluorescence microscopy (LSFM) for the quantitative imaging of cells and tissues, Cell Tissue Res. 360 (1) (2015) 129–141.
[41] E.G. Reynaud, J. Peychl, J. Huisken, P. Tomancak, Guide to light-sheet microscopy for adventurous biologists, Nat. Methods 12 (2014) 30.
[42] O.E. Olarte, J. Andilla, E.J. Gualda, P. Loza-Alvarez, Light-sheet microscopy: a tutorial, Adv. Opt. Photon. 10 (1) (2018) 111–179.
[43] J. Lim, H.K. Lee, W. Yu, S. Ahmed, Light sheet fluorescence microscopy (LSFM): past, present and future, Analyst 139 (19) (2014) 4758–4768.
[44] E.J. Gualda, D. Simão, C. Pinto, P.M. Alves, C. Brito, Imaging of human differentiated 3D neural aggregates using light sheet fluorescence microscopy, Front. Cell. Neurosci. 8 (221) (2014).
[45] M. Dobosz, V. Ntziachristos, W. Scheuer, S. Strobel, Multispectral fluorescence ultramicroscopy: three-dimensional visualization and automatic quantification of tumor morphology drug penetration, and antiangiogenic treatment response, Neoplasia 16 (1) (2014) 1–W7.
[46] L. Li, Q. Zhou, T.C. Voss, K.L. Quick, D.V. LaBarbera, High-throughput imaging: focusing in on drug discovery in 3D, Methods 96 (2016) 97–102.
[47] M. Zanoni, F. Piccinini, C. Arienti, A. Zamagni, S. Santi, R. Polico, A. Bevilacqua, A. Tesei, 3D tumor spheroid models for in vitro therapeutic screening: a systematic approach to enhance the biological relevance of data obtained, Sci. Reports 6 (2016) 19103.
[48] C. Wenzel, B. Riefke, S. Gründemann, A. Krebs, S. Christian, F. Prinz, M. Osterland, S. Golfier, S. Räse, N. Ansari, M. Esner, M. Bickle, F. Pampaloni, C. Mattheyer, E.H. Stelzer, K. Parczyk, S. Prechtl, P. Steigemann, 3D high-content screening for the identification of compounds that target cells in dormant tumor spheroid regions, Exp. Cell Res. 323 (1) (2014) 131–143.
[49] T. Bruns, S. Schickinger, H. Schneckenburger, Single plane illumination module and micro-capillary approach for a wide-field microscope, J. Vis. Exp. 90 (2014) 51993.
[50] G. Lazzari, V. Nicolas, M. Matsusaki, M. Akashi, P. Couvreur, S. Mura, Multicellular spheroid based on a triple co-culture: a novel 3D model to mimic pancreatic tumor complexity, Acta Biomater. 78 (2018) 296–307.
[51] J. Carlsson, J.M. Yuhas, Liquid-overlay culture of cellular spheroids, Recent Results Cancer Res. 95 (1984) 1–23.
[52] M. Matsusaki, H. Ajiro, T. Kida, T. Serizawa, M. Akashi, Layer-by-layer assembly through weak interactions and their biomedical applications, Adv. Mater. 24 (4) (2012) 454–474.

[53] J. Nicolas, Drug-initiated synthesis of polymer prodrugs: combining simplicity and efficacy in drug delivery, Chem. Mater. 28 (6) (2016) 1591–1606.
[54] S. Harrisson, J. Nicolas, A. Maksimenko, D.T. Bui, J. Mougin, P. Couvreur, Nanoparticles with in vivo anticancer activity from polymer prodrug amphiphiles prepared by living radical polymerization, Angew. Chem. Int. Ed. 52 (6) (2013) 1678–1682.
[55] Y. Guillaneuf, P.-E. Dufils, L. Autissier, M. Rollet, D. Gigmes, D. Bertin, Radical chain end chemical transformation of SG1-based polystyrenes, Macromolecules 43 (1) (2009) 91–100.
[56] D. Vinciguerra, S. Denis, J. Mougin, M. Jacobs, Y. Guillaneuf, S. Mura, P. Couvreur, J. Nicolas, A facile route to heterotelechelic polymer prodrug nanoparticles for imaging, drug delivery and combination therapy, J. Control. Release 286 (2018) 425–438.
[57] D. Vinciguerra, M. Jacobs, S. Denis, J. Mougin, Y. Guillaneuf, G. Lazzari, C. Zhu, S. Mura, P. Couvreur, J. Nicolas, Heterotelechelic polymer prodrug nanoparticles: adaptability to different drug combinations and influence of the dual functionalization on the cytotoxicity, J. Control. Release 295 (2019) 223–236.
[58] H. Fessi, F. Puisieux, J.P. Devissaguet, N. Ammoury, S. Benita, Nanocapsule formation by interfacial polymer deposition following solvent displacement, Int. J. Pharma. 55 (1) (1989) R1–R4.
[59] J. Swoger, P. Verveer, K. Greger, J. Huisken, E.H.K. Stelzer, Multi-view image fusion improves resolution in three-dimensional microscopy, Opt. Exp. 15 (13) (2007) 8029–8042.
[60] C.F. Thorn, C. Oshiro, S. Marsh, T. Hernandez-Boussard, H. McLeod, T.E. Klein, R.B. Altman, Doxorubicin pathways: pharmacodynamics and adverse effects, Pharmacogenet. Genomics 21 (7) (2011) 440–446.
[61] J. Huisken, D.Y.R. Stainier, Even fluorescence excitation by multidirectional selective plane illumination microscopy (mSPIM), Opt. Lett. 32 (17) (2007) 2608–2610.
[62] F. Pampaloni, U. Berge, A. Marmaras, P. Horvath, R. Kroschewski, E.H.K. Stelzer, Tissue-culture light sheet fluorescence microscopy (TC-LSFM) allows long-term imaging of three-dimensional cell cultures under controlled conditions, Integr. Biol. 6 (10) (2014) 988–998.
[63] S. Preibisch, S. Saalfeld, J. Schindelin, P. Tomancak, Software for bead-based registration of selective plane illumination microscopy data, Nat. Methods 7 (2010) 418.
[64] A. Gabizon, S. Amselem, D. Goren, R. Cohen, S. Druckmann, I. Fromer, R. Chisin, T. Peretz, A. Sulkes, Y. Barenholz, Preclinical and clinical experience with a doxorubicin-liposome preparation, J Liposome Res. 1 (4) (1990) 491–502.
[65] A. Gabizon, H. Shmeeda, Y. Barenholz, Pharmacokinetics of Pegylated Liposomal Doxorubicin, Clin. Pharmacokinet. 42 (5) (2003) 419–436.
[66] H.S. Yoo, E.A. Lee, T.G. Park, Doxorubicin-conjugated biodegradable polymeric micelles having acid-cleavable linkages, J. Control. Release 82 (1) (2002) 17–27.
[67] T. Nakanishi, S. Fukushima, K. Okamoto, M. Suzuki, Y. Matsumura, M. Yokoyama, T. Okano, Y. Sakurai, K. Kataoka, Development of the polymer micelle carrier system for doxorubicin, J. Control. Release 74 (1) (2001) 295–302.
[68] H.S. Yoo, K.H. Lee, J.E. Oh, T.G. Park, In vitro and in vivo anti-tumor activities of nanoparticles based on doxorubicin–PLGA conjugates, J. Control. Release 68 (3) (2000) 419–431.
[69] H. Cabral, Y. Matsumoto, K. Mizuno, Q. Chen, M. Murakami, M. Kimura, Y. Terada, M.R. Kano, K. Miyazono, M. Uesaka, N. Nishiyama, K. Kataoka, Accumulation of sub-100 nm polymeric micelles in poorly permeable tumours depends on size, Nat. Nanotechnol. 6 (2011) 815.